Received: 6 May 2023 | Revised: 18 September 2023 | Accepted: 27 September 2023

DOI: 10.1002/jev2.12371

RESEARCH ARTICLE

Engineered small extracellular vesicle-mediated NOX4 siRNA delivery for targeted therapy of cardiac hypertrophy

Ji-Young Kang[1] | Dasom Mun[1] | Yumin Chun[1] | Da-Seul Park[1] | Hyoeun Kim[2] | Nuri Yun[3] | Boyoung Joung[1,4]

[1]Division of Cardiology, Department of Internal Medicine, Yonsei University College of Medicine, Seodaemun-gu, Seoul, Republic of Korea

[2]Department of Biochemistry and Molecular Biology, Yonsei University College of Medicine, Seodaemun-gu, Seoul, Republic of Korea

[3]GNTPharma Science and Technology Center for Health, Giheung-gu, Yongin-si, Incheon, Republic of Korea

[4]Graduate School of Medical Science, Brain Korea 21 Project, Yonsei University College of Medicine, Seodaemun-gu, Seoul, Republic of Korea

Correspondence
Boyoung Joung, Division of Cardiology, Yonsei University College of Medicine, Seoul 03722, Republic of Korea. Email: cby6908@yuhs.ac

Nuri Yun, GNTPharma Science and Technology Center for Health, Gyeonggi-do 17096, Republic of Korea. Email: yunnuri@hanmail.net

Funding information
Ministry of Education, Grant/Award Number: 2021R1I1A1A01052197; Korean Cardiac Research Foundation, Grant/Award Number: 202101-02; Ministry of Science and ICT, Grant/Award Number: 2023R1A2C3003320; Ministry of Science and ICT, Ministry of Health & Welfare, Grant/Award Number: 21B0604L1

Abstract
Small-interfering RNA (siRNA) therapy is considered a powerful therapeutic strategy for treating cardiac hypertrophy, an important risk factor for subsequent cardiac morbidity and mortality. However, the lack of safe and efficient in vivo delivery of siRNAs is a major challenge for broadening its clinical applications. Small extracellular vesicles (sEVs) are a promising delivery system for siRNAs but have limited cell/tissue-specific targeting ability. In this study, a new generation of heart-targeting sEVs (CEVs) has been developed by conjugating cardiac-targeting peptide (CTP) to human peripheral blood-derived sEVs (PB-EVs), using a simple, rapid and scalable method based on bio-orthogonal copper-free click chemistry. The experimental results show that CEVs have typical sEVs properties and excellent heart-targeting ability. Furthermore, to treat cardiac hypertrophy, CEVs are loaded with NADPH Oxidase 4 (NOX4) siRNA (siNOX4). Consequently, CEVs@siNOX4 treatment enhances the in vitro anti-hypertrophic effects by CEVs with siRNA protection and heart-targeting ability. In addition, the intravenous injection of CEVs@siNOX4 into angiotensin II (Ang II)-treated mice significantly improves cardiac function and reduces fibrosis and cardiomyocyte cross-sectional area, with limited side effects. In conclusion, the utilization of CEVs represents an efficient strategy for heart-targeted delivery of therapeutic siRNAs and holds great promise for the treatment of cardiac hypertrophy.

KEYWORDS
cardiac hypertrophy, cardiac-targeting peptide, NADPH oxidase 4, small extracellular vesicles, small-interfering RNA

1 | INTRODUCTION

Cardiac hypertrophy is an independent risk factor for cardiac morbidity and mortality and plays a critical role in the cardiovascular system (Shimizu & Minamino, 2016; Yang et al., 2020). An adaptive response to various physiological or pathological stimuli, cardiac hypertrophy is characterized by enlargement of cardiomyocyte size, reactivation of foetal genes and reorganization of cytoskeleton (Lu et al., 2016). Although cardiac hypertrophy is initially a compensatory mechanism for maintaining cardiac function, sustained hypertrophy can ultimately lead to irreversible structural cardiac remodelling and impaired cardiac function, eventually resulting in heart failure, arrhythmia and sudden death (Berk et al., 2007; Dorn et al., 2003; Hill & Olson, 2008; Ruwhof & van der Laarse, 2000). However, there are no effective treatments for cardiac hypertrophy (Frey et al., 2004;

Li et al., 2020). Therefore, novel therapeutic approaches and drugs for the treatment of cardiac hypertrophy should be urgently developed.

Small-interfering RNA (siRNA) therapy, which is based on specific post-transcriptional gene silencing, is currently one of the most promising therapeutic platforms for the treatment of cardiovascular diseases, including cardiac hypertrophy (Goyal et al., 2009; Poller et al., 2013; Raghunathan & Patel, 2013; Shah & Giacca, 2022). Nevertheless, there exist certain issues in siRNA delivery, including poor blood stability, safety and cellular uptake, which are the key barriers in wide application of siRNA therapy (Reischl & Zimmer, 2009; Tatiparti et al., 2017). Over the past few decades, viral vectors, synthetic polymeric nanoparticles and liposomes have been the most commonly studied carriers for siRNA delivery (Kanasty et al., 2013; Lamberti & Barba, 2020; Whitehead et al., 2009). However, several drawbacks, such as the risk of immunogenicity and mutagenic toxicity, poor biocompatibility and low efficiency, limit the use of these carriers for siRNA delivery (Liang et al., 2022; Lu et al., 2018; Zu & Gao, 2021). Therefore, more efficient and better tolerated approaches for improving the delivery efficiency of siRNAs are urgently needed.

Small extracellular vesicles (sEVs) are a type of extracellular vesicle with a diameter of 30−200 nm that are secreted by various types of cells into the extracellular fluid of blood, urine and saliva (Colombo et al., 2014; Shah et al., 2018; Théry et al., 2018). In addition, sEVs facilitate the transport of bioactive molecules such as nucleic acids, proteins and lipids from their parental cells to the recipient cells, thus playing important roles in cell-to-cell communication (Colombo et al., 2014; Mathivanan et al., 2010; Théry et al., 2002). Recently, increasing attention has been paid to the use of sEVs as nanocarriers for siRNA delivery (Lu et al., 2018; Walker et al., 2019). As natural carriers, sEVs offer several favourable features, such as low toxicity and immunogenicity, high stability in circulation, intrinsic ability to cross biological barriers and strong cargo loading and protection capacity compared with conventional carriers. (El Andaloussi et al., 2013; Vader et al., 2016; Zhu et al., 2022). However, a great challenge in sEV-based delivery carriers is that after systemic administration, sEVs are likely to accumulate in non-specific organs, especially in the liver, leading to insufficient delivery to the specific target cell/tissue (Lai et al., 2014; Wiklander et al., 2015).

Numerous studies have reported that the targeting efficiency of sEVs can be improved through surface modification with specific cell/tissue-targeting peptides (Murphy et al., 2019; Ramasubramanian et al., 2019). Notably, the most popular method is cell engineering, in which donor cells are engineered to release specific cell/tissue-targeting peptide-conjugated sEVs (Alvarez-Erviti et al., 2011; Kim et al., 2018). However, these processes are complex and time-consuming and cannot be readily applied to pre-isolated sEVs or sEVs from body fluids. (Armstrong et al., 2017; Kooijmans et al., 2016). Hence, it is imperative to modify sEVs using biochemical methods that can be applied easily and efficiently. Recent studies have demonstrated an efficient strategy to simply and rapidly modify the surface of sEVs with different cell/tissue-targeting peptides using bio-orthogonal copper-free click chemistry (Hao et al., 2022; Tian et al., 2022; Zhu et al., 2018). For example, Tian et al. developed c(RGDyK)-conjugated sEVs as targeted delivery vehicles to the ischemic brain (Tian et al., 2018). In addition, Wang et al. generated hypertensive pulmonary artery-targeted sEVs by conjugating the CAR (CARSKNKDC) peptide to sEVs for pulmonary hypertension therapy (Wang et al., 2020). However, the sEVs currently modified via bio-orthogonal copper-free click chemistry are mostly designed to treat tumours or cerebrovascular disease.

In this study, we designed a highly efficient heart-targeting delivery system by conjugating sEVs with a cardiac-targeting peptide (CTP) that exhibits cell-targeting specificity for cardiomyocytes, using bio-orthogonal copper-free click chemistry (Avula et al., 2012, 2015; Zahid et al., 2010). Interestingly, the original sEVs were derived from human peripheral blood, which is a reliable and easily adaptable source of sEVs. Additionally, we loaded CTP-modified functional sEVs (CEVs) with cholesterol-modified NADPH Oxidase 4 (NOX4) siRNA (siNOX4), which has been identified as a molecular target for treating cardiac hypertrophy. Our results showed that CEVs@siNOX4 possess enhanced heart-targeting ability, effectively attenuating angiotensin II (Ang II)-induced NOX4 expression in human induced pluripotent stem cell-derived ventricular cardiomyocytes (iPSC-vCMs). Consequently, CEVs@siNOX4 led to significant decrease in cell surface area and downregulation of hypertrophic markers (ANP, BNP and β-MHC). In addition, a series of in vivo experiments showed that the systemic administration of CEVs@siNOX4 exerted strong cardioprotective effects in Ang II-treated mice. Therefore, our study provides a proof-of-concept for an sEV-based therapeutic strategy that enables efficient and specific delivery of siRNA for cardiac hypertrophy-targeted therapy.

2 | MATERIALS AND METHODS

2.1 | Cell culture and Ang II treatment

HEK293 (Korean Cell Line Bank, Seoul, Korea), AC16, and H9C2 cells (ATCC, Rockville, MD, USA) were cultured in Dulbecco's modified eagle medium (DMEM; LM001-05, Welgene, Gyeongsan, Korea) supplemented with 10% foetal bovine serum (FBS; US-FBS-500, Young In Frontier, Seoul, Korea) and 1% penicillin-streptomycin (10378016, Gibco, Grand Island, NY, USA) at 37°C in a humidified atmosphere with 5% CO_2.

The human induced pluripotent stem cell (iPSC) line CMC-hiPSC-011 was provided by the Korea National Stem Cell Bank, originally provided by Catholic University. iPSCs were differentiated into iPSC-vCMs and iPSC-derived atrial cardiomyocytes (iPSC-aCMs), as previously described with slight modifications (Cyganek et al., 2018; Maas et al., 2021). Briefly, iPSCs

differentiation was initiated at 80%−90% confluence in Matrigel (354277, Corning, Arizona, USA)-coated plates with cardio differentiation medium composed of RPMI 1640 (11875119, Thermo Fisher Scientific, Waltham, MA, USA) supplemented with B-27 minus insulin (A1895601, Thermo Fisher Scientific) and sequential treatment with 2 μM CHIR99021 (4423, Tocris Bioscience, Bristol, UK) for 72 h and then 2 μM Wnt-C59 (5148, Tocris Bioscience) for 48 h. The medium was replaced with cardio culture medium composed of RPMI 1640 supplemented with B-27 (17504001, Thermo Fisher Scientific) on day 9. For atrial subtype differentiation, 1 μM retinoic acid (RA; R2625, Sigma-Aldrich; Merck KGaA, Darmstadt, Germany) was supplemented from days 4 to 7.

To establish cardiac hypertrophy in vitro, iPSC-vCMs were treated with 2.5 μM Ang II (A9525; Sigma-Aldrich; Merck KGaA) for 48 h.

2.2 | Preparation of CEVs

Human peripheral blood was obtained from five patients without serious or progressive cardiovascular diseases at the Yonsei University Health System (Seoul, Korea) from August 2018 to July 2021. Written informed consent was obtained from all patients. The clinical profiles of the patients are presented in Table S1. The study was approved by the local ethics committee (Institutional Review Board of Severance Hospital (Seoul, Korea) of the Yonsei University Health System; approval no. 4-2011-0872 and 4-2019-0620) and adhered to the tenets of the Declaration of Helsinki. sEVs were isolated from human peripheral blood using differential ultracentrifugation. Briefly, human peripheral blood was centrifuged at 300 × *g* for 10 min, 2000 × *g* for 10 min and 10,000 × *g* for 30 min and then filtered using a 0.22 μm pore-size filter (Merck Millipore, Tullagreen, Ireland). Subsequently, the filtrate was ultracentrifuged at 100,000 × *g* for 1 h, and the pelleted sEVs were resuspended in PBS and ultracentrifuged again at 100,000 × *g* for 1 h. The final pellet was resuspended in PBS, aliquoted to avoid freeze and thaw cycles, and stored at −80°C.

CEVs were constructed by conjugating CTP to human peripheral blood-derived sEVs (PB-EVs) in a two-step reaction. First, 0.5 μg/μL sEVs in PBS was incubated with 3 μM dibenzylcyclooctyne-sulfo-*N*-hydroxysuccinimidyl ester (DBCO-sulfo-NHS; 762040, Sigma-Aldrich; Merck KGaA) for 4 h at room temperature (RT). Unconjugated DBCO-sulfo-NHS was removed by three washes with Amicon® Ultra Centrifugal Filters (UFC8010, Merck Millipore). The DBCO-conjugated sEVs were then linked to the azide-containing peptides using bio-orthogonal copper-free click chemistry. Scrambled peptide (Scr; 5′-azide-ARPLEHGSDKAT) and CTP (5′-azide-APWHLSSQYSRT) with azide groups were synthesized by Peptron (Daejeon, Korea). Next, 0.3 μM Scr or CTP was added to DBCO-conjugated sEVs, and 0.3 μM Cy5.5-azide (Lumiprobe Corp., Hallandale Beach, FL, USA) was subsequently added for imaging studies. The reaction was conducted on a rotating mixer for 12 h at 4°C. To remove unincorporated peptides, sEVs were washed thrice with PBS using Amicon® Ultra Centrifugal Filters (UFC8010, Merck Millipore). After washing with PBS, the modified sEVs were resuspended and stored at −80°C for subsequent experiments.

To confirm successful CTP conjugation to PB-EVs, tetramethyl rhodamine (TAMRA)-labelled CTP with an azide group was synthesized by Peptron (Daejeon, Korea) and loaded onto PB-EVs by the same reaction as for CEVs modification. The sEVs were solubilized using 0.5% Triton X-100 (93443, Sigma-Aldrich; Merck KGaA) and subjected to fluorescence analysis. A standard curve of free TAMRA-labelled CTP was used to calculate the concentration of CTP in PB-EVs.

2.3 | Characterization of sEVs

For performing transmission electron microscopy (TEM), sEVs were added onto a formvar-carbon-coated electron microscopy grid (Leica Microsystems, Inc., Buffalo Grove, IL, USA) and stained with 2% uranyl acetate. The morphology of sEVs was observed using a JEM-1011 (JEOL Ltd., Tokyo, Japan).

Nanoparticle tracking analysis (NTA) was performed using the NanoSight LM10 instrument (Malvern Instruments Ltd., Malvern, UK). The Brownian motion of sEVs was recorded and captured for 60 s at RT and analysed using NTA v.2.3 software (Malvern Panalytical, Ltd.) by applying the Stokes–Einstein equation.

After the sEVs were diluted to 1:5000 in PBS, zeta potential analysis was performed to determine the surface charge of the sEVs using an ELS-1000ZS (Otsuka Electronics, Osaka, Japan).

2.4 | Measurement of sEVs uptake in vitro and in avivo

Modified sEVs were labelled using the PKH67 Green Fluorescent Cell Linker Kit (PKH67GL, Sigma-Aldrich; Merck KGaA) according to the manufacturer's instructions. After incubation with PKH67-labelled CEVs for 24 h, the cells were washed thrice with PBS, fixed with 4% paraformaldehyde, and observed using a confocal microscopy (Zeiss LSM 710, Carl Zeiss). Nuclei were stained with Hoechst 33342 (H3570, Thermo Fisher Scientific).

To determine in vivo distribution of modified sEVs, mice were intravenously injected with each sEVs sample. After 24 h of intravenous injection, Cy 5.5 fluorescence signals in the dissected organs (heart, liver, spleen, lung and kidneys) were captured using an IVIS® spectrum in vivo imaging system (PerkinElmer, Waltham, MA, USA).

In addition, heart tissues were cryosectioned 24 h post-injection and immunofluorescent stained with anti-cardiac troponin I (cTnI; ab47003, Abcam, Cambridge, U.K), anti-von Willebrand factor (vVF; ab6994, Abcam), or anti-vimentin (ab92547, Abcam). The slides were then stained with 4′,6-diamidino-2-phenylindole (DAPI; 62248, Thermo Fisher Scientific) and observed using a confocal microscopy (Zeiss LSM 710, Carl Zeiss).

2.5 | Loading of siRNA into CEVs

The scrambled siRNA (siCtrl) and siNOX4 modified with 2′-*O*-methyl and conjugated with cholesterol at the 3′ end were synthesized by Bioneer (Daejeon, Korea). To load siRNA into sEVs, these siRNAs (1 nmol) were incubated with SEVs or CEVs (100 μg/mL) at 37°C for 1 h. Next, they were washed with PBS using Amicon® Ultra Centrifugal Filters (UFC8010, Merck Millipore). The sEVs were used directly in further experiments. To estimate the concentration of siRNA loaded onto the sEVs, FAM-labelled and cholesterol-conjugated siCtrl were synthesized and loaded onto the sEVs. The sEVs were solubilized using 0.5% Triton X-100 (93443, Sigma-Aldrich; Merck KGaA) and subjected to fluorescence analysis. A standard curve of free FAM-labelled siCtrl was used to calculate the siRNA concentration in the sEVs.

2.6 | Measurement of toxicity in vitro and in vivo

To determine toxicity in vitro, cell viability and LDH release were examined using Quint-MAX™ WST-8 cell viability assay kit (QM2500, Biomax, Seoul, Korea) and Quint-LDH™ PLUS cytotoxicity assay kit (BCT-LDHP1000, Biomax) according to the manufacturer's instructions, respectively. The absorbance was measured at 450 nm using a microplate reader (VersaMax, Molecular Devices, Sunnyvale, CA, USA).

The concentrations of interleukin-6 (IL-6), interleukin-10 (IL-10), interferon-γ (IFN-γ) and tumour necrosis factor-α (TNF-α) in serum from mice were quantified using enzyme-linked immunosorbent assay (ELISA) kit for IL-6 (88-7064-22, Thermo Fisher Scientific), IL-10 (88-7105-22, Thermo Fisher Scientific), IFN-γ (88-7314-22, Thermo Fisher Scientific) and TNF-α (88-7324-22, Thermo Fisher Scientific) according to the manufacturer's instructions, respectively. The absorbance was measured at 450 nm using a microplate reader (VersaMax, Molecular Devices). In addition, the dissected tissues (heart, liver, spleen, lung and kidneys) were fixed in 4% paraformaldehyde, embedded in paraffin, and sliced into 4-μm thick sections. The sections were stained with hematoxylin and eosin (H&E) and observed under an inverted microscope (Olympus, Tokyo, Japan).

2.7 | Cell transfection

The negative control and NOX4 siRNA were synthesized by Bioneer (Daejeon, Korea). After iPSC-vCMs had reached approximately 60%–80% confluency, the cells were transfected with Lipofectamine™ RNAiMAX (13778150, Thermo Fisher Scientific) according to the manufacturer's instructions and harvested for subsequent analyses.

2.8 | Measurement of cardiomyocyte size

iPSC-vCMs were fixed with 4% paraformaldehyde, permeabilized with 0.3% Triton-X100/PBS, and blocked with 1% bovine serum albumin (BSA)/PBS. The cells were then incubated with fluorescence-conjugated α-actinin antibody (sc-17829, 1:200; Santa Cruz Biotechnology Inc., Dallas, TX, USA) overnight at 4°C. After five washes with PBS, the nuclei were stained with Hoechst 33342 (H3570, Thermo Fisher Scientific). The cells were observed using a confocal microscopy (Zeiss LSM 710, Carl Zeiss).

2.9 | Quantitative reverse transcription polymerase chain reaction (qRT-PCR)

Total RNA was isolated using miRNeasy® Mini Kit (217004, Qiagen, Hilden, Germany) and reverse transcribed into cDNA using High-Capacity cDNA Reverse Transcription Kit (4368814, Applied Biosystems, Darmstadt, Germany) according to the manufacturer's instructions. qRT-PCR was performed using PowerUp™ SYBR™ Green Master Mix (A25742, Applied Biosystems) on an AriaMx Realtime PCR System (Agilent Technologies, USA). The relative expression of mRNA was calculated according to

the $2^{-\Delta\Delta Cq}$ method and normalized against GAPDH (Livak & Schmittgen, 2001). The PCR primers were synthesized by Cosmo Genetech (Daejeon, Korea) and are listed in Table S2.

2.10 | Western blot analysis

Total protein was extracted by radioimmunoprecipitation assay buffer supplemented with protease and phosphatase inhibitors (WSE-7420, ATTO, Tokyo, Japan), and the protein concentration was determined using Pierce™ 660 nm Protein Assay Reagent (22660, Thermo Fisher Scientific). Equal amounts of protein were separated by 10% sodium dodecyl sulphate polyacrylamide gel electrophoresis (SDS-PAGE) and transferred onto polyvinylidene fluoride membranes (IPVH00010, EMD Millipore, Bedford, MA, USA). The membranes were then blocked with 5% BSA in TBS-Tween 20 (TBS-T) and incubated overnight at 4°C with the following primary antibodies: Alix (sc-53540, 1:1,000; Santa Cruz Biotechnology Inc.), TSG101 (sc-7964, 1:1,000; Santa Cruz Biotechnology Inc.), CD81 (sc-166029, 1:1,000; Santa Cruz Biotechnology Inc.), NOX4 (ab133303, 1:500; Abcam) and β-actin (sc-47778, 1:1,000; Santa Cruz Biotechnology Inc.). After incubation with horseradish peroxidase-conjugated secondary antibodies (sc-516102, sc-2357, 1:5000; Santa Cruz Biotechnology Inc.), signals were visualized using an enhanced chemiluminescence kit (1705061, Bio-Rad Laboratories Inc., Hercules, CA, USA).

2.11 | Identification and functional analysis of target genes

The gene expression profiles of GSE41177, GSE79768 and GSE115574 were downloaded from Gene Expression Omnibus (GEO, https://www.ncbi.nlm.nih.gov/geo/), a public functional genomics data repository. After integrating the three datasets, differentially expressed genes (DEGs) between patients with sinus rhythm (SR) and those with AF were analysed using the limma R package (version 3.52.2) (Ritchie et al., 2015). DisGeNET (https://www.disgenet.org), a discovery platform integrating gene–disease associations, was used to select the set of genes associated with AF. In addition, gene ontology (GO) and KEGG pathway enrichment analyses were performed using Database for Annotation, Visualization and Integrated Discovery (DAVID, https://david.ncifcrf.gov). Gene ontology biological processes (GOBP) and KEGG pathways with $P < 0.05$ were considered to be significantly enriched. To construct the protein-protein interaction (PPI) network, we used Search Tool for the Retrieval of Interacting Genes (STRING; https://string-db.org) and Cytoscape software (version 3.8.0).

2.12 | Animal experiments

All experimental animal procedures were performed in accordance with the ethical approval of the Institutional Animal Care and Use Committee of the Yonsei University College of Medicine (approval no. 2021-0152) and the Guide for the Care and Use of Laboratory Animals published by the US National Institutes of Health (Publication No. 85-23, revised 1996). C57BL/6 male mice were purchased from Orient Bio Inc. (Seongnam, Korea) and maintained at standard conditions (temperature, 20 ± 0.5°C; humidity, 60 ± 5%; light/dark cycle, 12 h). The mice were anesthetized with intraperitoneal injections of tiletamine-zolazepam (Zoletil 50, 30 mg/kg) and xylazine (Rompun®, 10 mg/kg) and implanted with Ang II-containing Alzet® 1002 micro-osmotic pumps (1.5 mg/kg/day; Durect Corp., Cupertino, CA, USA). The control mice were implanted with PBS-containing Alzet® 1002 micro-osmotic pumps.

To evaluate cardiac function, echocardiography was performed using the Vevo 2100 system (VisualSonics, Toronto, Ontario, Canada). Left ventricular ejection fraction (LVEF) and left ventricular fractional shortening (LVFS) were calculated as follows: LVEF (%) = [(left ventricular end-diastolic volume (LVEDV) – left ventricular end-systolic volume (LVESV))/LVEDV] × 100; LVFS (%) = [(left ventricular end-diastolic diameter (LVEDD) – left ventricular end-systolic diameter (LVESD))/LVEDD] × 100.

For histological examination, heart tissues were fixed in 4% paraformaldehyde, embedded in paraffin and sliced into 4-μm thick sections. The slides were stained with H&E and Masson's trichrome (MT) and observed under an inverted microscope (Olympus, Japan). In addition, the slides were stained with wheat germ agglutinin (WGA) conjugated to Alexa Fluor 488 (W11261, Thermo Fisher Scientific) to evaluate cross-sectional area (CSA). The fibrotic area and CSA were quantified using the ImageJ 1.50i software (National Institutes of Health, Bethesda, MD, USA).

2.13 | Statistical analysis

All data are presented as the mean ± standard error of the mean. Comparisons between two groups were performed using a two-tailed Student's *t*-test, and multiple groups were compared using a one-way analysis of variance (ANOVA) with Tukey's post

hoc test. All statistical analyses were performed using GraphPad Prism (version 8.42), and $P < 0.05$ was considered statistically significant.

3 | RESULTS

3.1 | Preparation and characterization of CEVs

We first isolated sEVs from human peripheral blood using ultracentrifugation (Figure S1A). The isolated sEVs were characterized based on morphology, diameter, protein markers and zeta potential using TEM, NTA, western blot analysis and electrophoretic light scattering (ELS), respectively. As expected, PB-EVs had a typical round-shape with a mean diameter of 138.7 ± 5.2 nm (Figure S1B and C). In addition, PB-EVs expressed sEV-specific markers, such as Alix, TSG101 and CD81, and had negative surface charges (Figure S1D and E). These results demonstrated that sEVs were successfully isolated from human peripheral blood.

Next, we determined the safety of PB-EVs in mice. These sEVs had no effect on the levels of IL-6, IL-10, IFN-γ and TNF-α, which are known as key cytokines of adaptive immunity (Iyer & Cheng, 2012; Schoenborn & Wilson, 2007; Tanaka et al., 2014; Yang et al., 2018), thereby implying that they did not activate adaptive immune response (Supplementary Figure S2A). In addition, there was no marked histological difference of H&E-stained major organs (heart, liver, spleen, lung and kidneys) in PB-EVs-injected mice, compared to PBS-injected mice (Figure S2B). Therefore, these results demonstrated that PB-EVs could potentially be used as a safe nanocarrier for siRNA delivery without obvious immunogenicity and toxicity.

To develop heart-targeting sEVs, we conjugated CTP onto PB-EVs surface using a previously described biochemical method (Figure 1a) (Tian et al., 2018). Briefly, DBCO groups were introduced on the surface of sEVs by cross-linking sEVs with DBCO-sulfo-NHS and reacting with azide-functionalized CTP to form stable triazole linkages using bio-orthogonal copper-free click chemistry. To track sEVs biodistribution, Cy5.5 azide was conjugated to their surfaces. Consequently, we obtained CTP-modified sEVs named CEVs. As a control, we prepared SEVs by conjugating azide-functionalized Scr to sEVs. To confirm the presence of CTP on the surface of PB-EVs, we conjugated TAMRA-labelled CTP to PB-EVs and assessed their fluorescence. By comparison to a standard fluorescence curve of free TAMRA-labelled CTP, 1 mg/mL CTP-modified sEVs was found to contain an average of 445 nM CTP (Figure S3). Therefore, these results showed that CTP was successfully conjugated to the surface of PB-EVs.

After preparation of CEVs, we confirmed whether the typical sEVs properties were maintained following surface modification of sEVs. TEM and NTA showed that both types of sEVs were spherical, with mean diameters ranging from 100 to 150 nm (Figure 1b and c). In addition, zeta potential of SEVs and CEVs were negative and distributed −17.0 ± 2.7 mV and −12.6 ± 1.3 mV, respectively (Figure 1d). Western blot analysis revealed that Alix, TSG101 and CD81 were enriched in both types of sEVs (Figure 1e). Thus, CTP conjugation maintains the integrity of sEVs. Both types of sEVs did not cause observable toxicity in the range of 5–100 μg/mL, as indicated by cell viability and LDH release assays (Figure 1f and g). Moreover, 7 days of storage at 4°C and 4 weeks of storage at −80°C had no significant effect on the mean diameter of CEVs (Figure 1h and i). Taken together, these results imply that CEVs could potentially be used for subsequent experiments.

3.2 | Targeting ability of CEVs in vitro and in vivo

To investigate whether CEVs exert cardiomyocyte-targeting ability in vitro, iPSC-vCMs, AC16 (immortalized human ventricular cardiomyocytes), H9C2 (immortalized rat embryonic cardiomyocytes), and HEK293 cells (immortalized human embryonic kidney cells) were incubated singly with CEVs. After 24 h of incubation, there was no significant difference in the uptake efficiency of SEVs and CEVs by HEK293 cells (Figure 2a). In contrast, CEVs were highly internalized by iPSC-vCMs compared with SEVs (Figure 2b). In addition, we showed that both AC16 and H9C2 cells efficiently taken up CEVs compared to SEVs (Figure 2c and d). Therefore, these results demonstrated that CEVs exhibit high specificity for cardiomyocytes in vitro.

Moreover, we evaluated in vivo distribution of CEVs. After 24 h of intravenous injection with PBS, SEVs, or CEVs in untreated or Ang II-treated mice, different organs of mice were dissected and quantitatively analysed by IVIS® spectrum in vivo imaging system. As shown in Figure 2e and Figure S5A, the fluorescence intensity in the heart injected with CEVs was approximately 2.0-fold greater than that in the heart injected with SEVs; however, there was no significant difference in the fluorescence intensity of other organs (liver, spleen, lung and kidneys) between the indicated groups (Figures S4 and S5B). In addition, the specific cell types targeted by CEVs were investigated by immunofluorescence staining of frozen heart sections for cTnI, vVF and vimentin, which are markers for cardiomyocytes, endothelial cells and cardiac fibroblasts, respectively. Interestingly, a high fluorescence signal was observed in cardiomyocytes compared to either endothelial cells or cardiac fibroblasts 24 h after intravenous injection of CEVs (Figure 2f). Collectively, these results indicated that CEVs had strong tropism for the heart, especially cardiomyocytes, both in vitro and in vivo, displaying their potential as a heart-targeted delivery system.

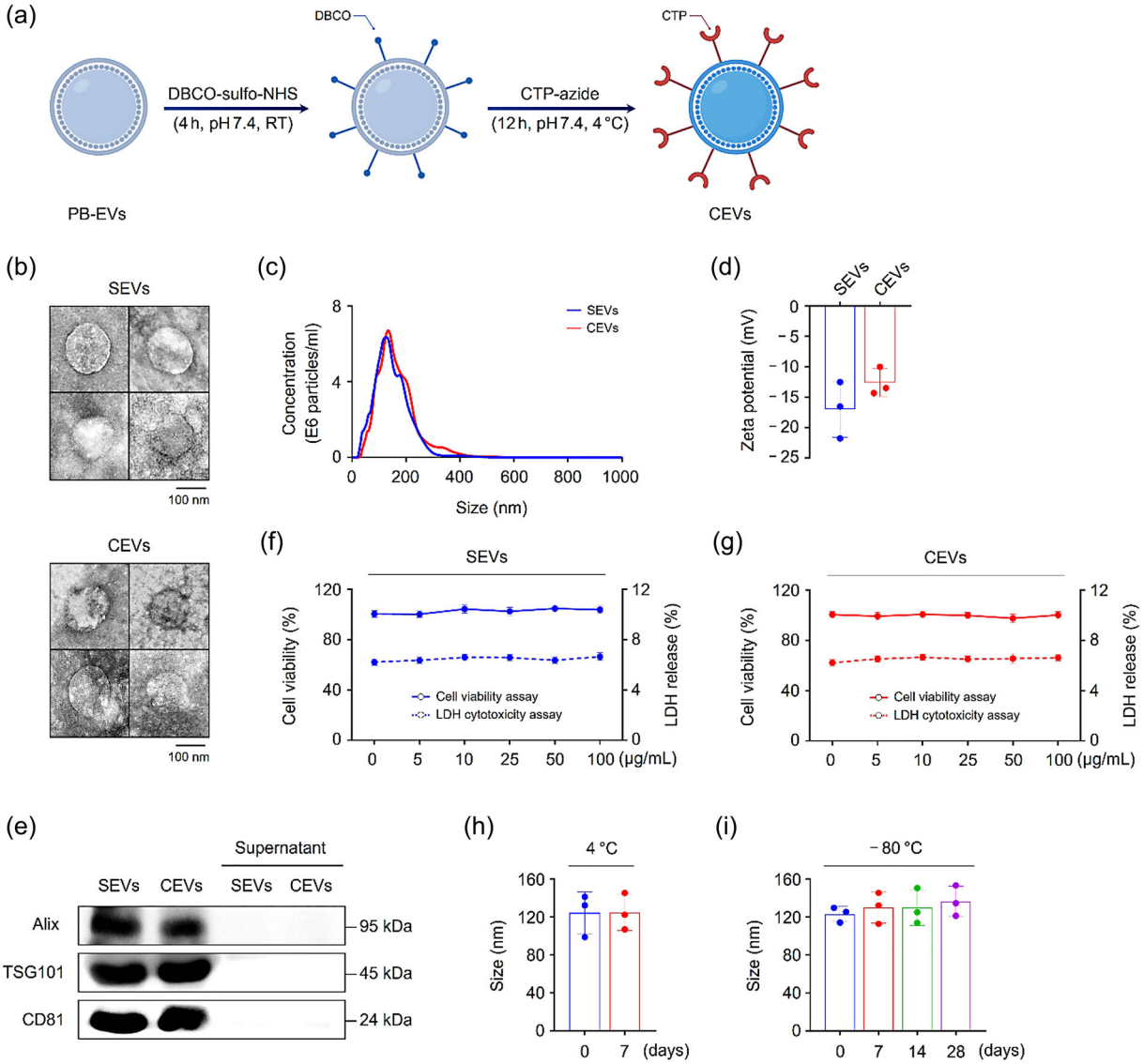

FIGURE 1 Characterization of CEVs and its toxicity in vitro. (a) Schematic diagram of CEVs generation by a two-step reaction. (b) Transmission electron micrograph of SEVs and CEVs. Scale bar = 100 nm. (c) Size distribution of SEVs and CEVs, as determined by NTA. (d) Zeta potential analysis of SEVs and CEVs. (e) Representative blots of Alix, TSG101 and CD81 in both types of sEVs. The supernatant was used as a negative control. Uncropped blots are shown in Figure S11. (f and g) The analysis of cell viability and LDH release in iPSC-vCMs treated with SEVs or CEVs. (h and i) Mean diameter of SEVs and CEVs stored at 4°C (h) and −80°C (i), determined by NTA.

3.3 | Identification of NOX4 as a molecular target of treating cardiac hypertrophy

After confirming heart-targeting ability of CEVs, we then attempted to investigate whether CEVs could effectively deliver siRNA and exert therapeutic effects; hence, we first selected a suitable siRNA candidate for subsequent experiments. Cardiac hypertrophy is a well-known risk factor of atrial fibrillation (AF) (Rosenberg et al., 2012). According to previous studies, the most common sustained arrhythmia in hypertrophic cardiomyopathy (HCM) is AF, affecting one in five patients, in whom it is associated with a markedly increased risk of stroke (MacIntyre & Lakdawala, 2016). Interestingly, recent studies have found that prolonged cardiac hypertrophy leads to progressive worsening of structural remodelling, thereby leading to AF (De Jong et al., 2011; Schoonderwoerd et al., 2005). In addition, it has been reported that cardiac hypertrophy-mediated electrical remodelling is linked to the pathogenesis of AF (Fu et al., 2019; Hill, 2003; Jansen et al., 2020). Therefore, the prevention of cardiac hypertrophy may be a potential approach for the treatment of AF; thus, we identified molecular profiles to characterize AF.

To investigate the differences in gene expression between patients with AF and SR, we analysed three independent GEO datasets (GSE41177, GSE79768 and GSE115574) (Figure 3a). After normalization and batch effect correction, a total of 434 genes were differentially expressed (150 downregulated and 284 upregulated) in patients with AF compared with their expression

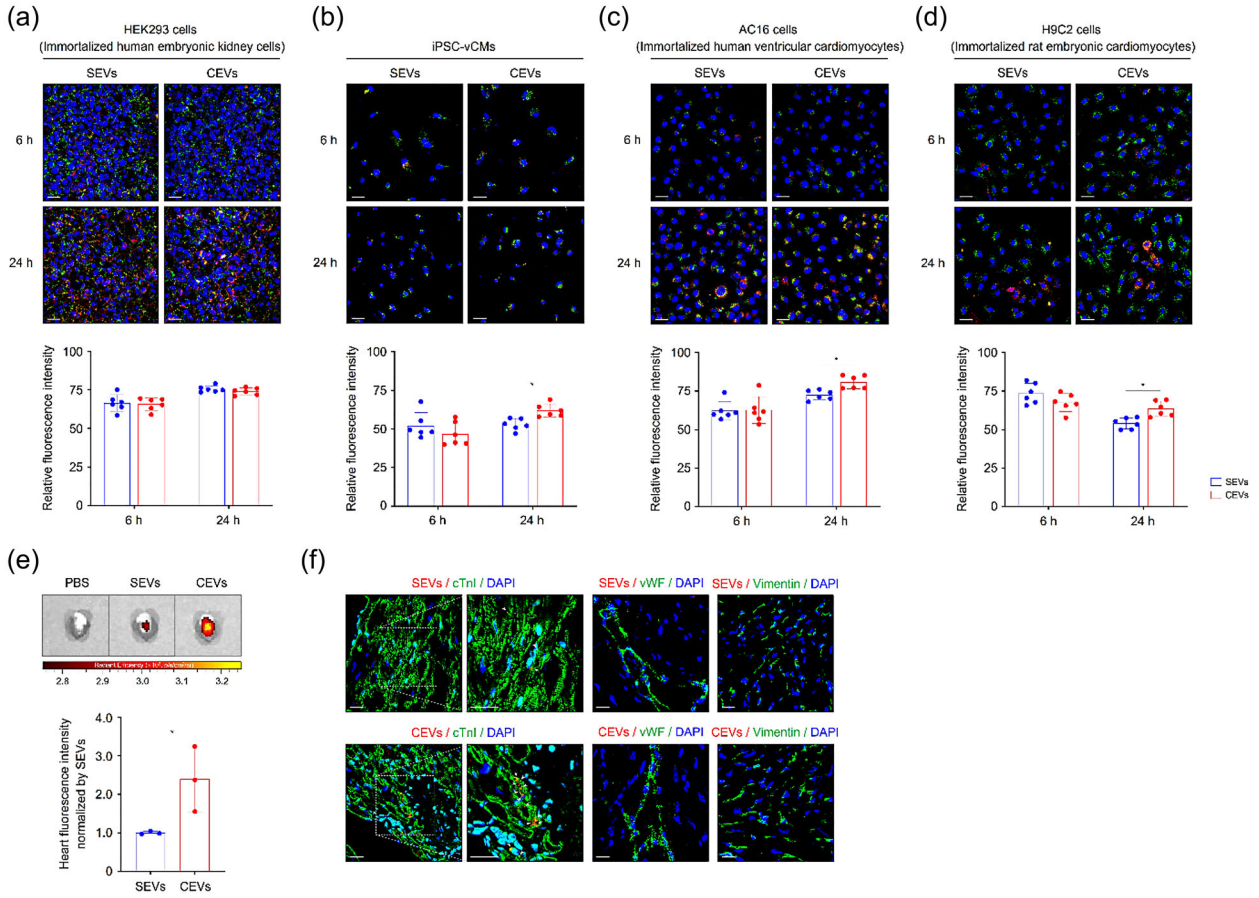

FIGURE 2 In vitro and in vivo heart-targeting ability of CEVs. (a–d) Representative immunofluorescence images and quantified data showing HEK293 cells, iPSC-vCMs, AC16 and H9C2 cells treated with PKH67 (green)-labelled SEVs and CEVs. Nuclei were stained with Hoechst 33342 (blue). Red fluorescence indicates Cy5.5-azide conjugated with the sEVs. Scale bar = 50 μm. (e) Representative IVIS images and quantified data showing fluorescence intensity in mice heart tissues at 24 h after intravenous injection of PBS, SEVs, or CEVs in untreated mice; $n = 3$ per group. (f) Representative immunofluorescence images of SEVs and CEVs internalized by cTnI$^+$ cardiomyocytes, vWF$^+$ endothelial cells, or vimentin$^+$ cardiac fibroblasts. Nuclei were stained with DAPI (blue); $n = 3$ per group. Scale bar = 20 μm. $^*P < 0.05$.

in patients with SR (log2|fold change| ≥ 0.58, $P < 0.05$), indicating distinct gene expression patterns between the two groups (Figure 3b). Among them, 36 DEGs overlapped with AF-associated genes identified from DisGeNET (Figure 3c) and are listed in Table S3. In addition, we explored the potential functions of these DEGs using GO and KEGG pathway enrichment analyses (Figure 3d). Consequently, these DEGs were significantly enriched in 77 GO terms. In particular, they are involved in the inflammatory response, cell adhesion, cardiac muscle cell contraction, apoptotic processes, wound healing and cellular responses to reactive oxygen species, which are associated with the development of cardiac hypertrophy. In addition, KEGG pathway enrichment analysis showed that these DEGs were enriched in cardiac hypertrophy-related pathways such as focal adhesion, regulation of the actin cytoskeleton, Rap1 signalling pathway, ECM-receptor interaction and MAPK signalling pathway. Therefore, these results suggested that these DEGs may contribute to cardiac hypertrophy in AF.

Notably, previous studies have shown that NOX4 is a key factor that contributes to cardiac hypertrophy, eventually resulting in AF (Ma et al., 2016; Matsushima et al., 2013). For example, Kuroda et al. demonstrated that in mice with cardiac-specific deletion of NOX4, cardiac hypertrophy was significantly attenuated (Kuroda et al., 2010). In addition, Zeng et al. showed that NOX4 promotes Ang II-induced cardiac hypertrophy through the reactive oxygen species/a disintegrant and metalloproteinase 17 pathways (Zeng et al., 2019). In consideration of previous studies, we selected NOX4 for subsequent experiments, even though NOX4 did not show the highest fold change among 36 DEGs.

As shown in Figure 3e, it was evident that NOX4 was associated with cardiac hypertrophy-associated genes such as NOS3, HMOX1, CAT, DECR1, CYBB, AKT1, AGER and SMAD3 in the STRING PPI network. In addition, to evaluate NOX4 levels in response to cardiac hypertrophy, we differentiated iPSCs into ventricular cardiomyocytes (iPSC-vCMs) (Figure S6A). As shown in Figure S6B, qRT-PCR analysis revealed that iPSC-vCMs expressed higher levels of ventricle-specific genes such as HEY2, MYH2 and MYH7, whereas the levels of atrial-specific genes such as GJA5, KCNA5, KCNJ3, MYL7 and NPPA in iPSC-vCMs were significantly lower than those in iPSC-aCMs. We then determined the concentration of Ang II required to induce hypertrophic

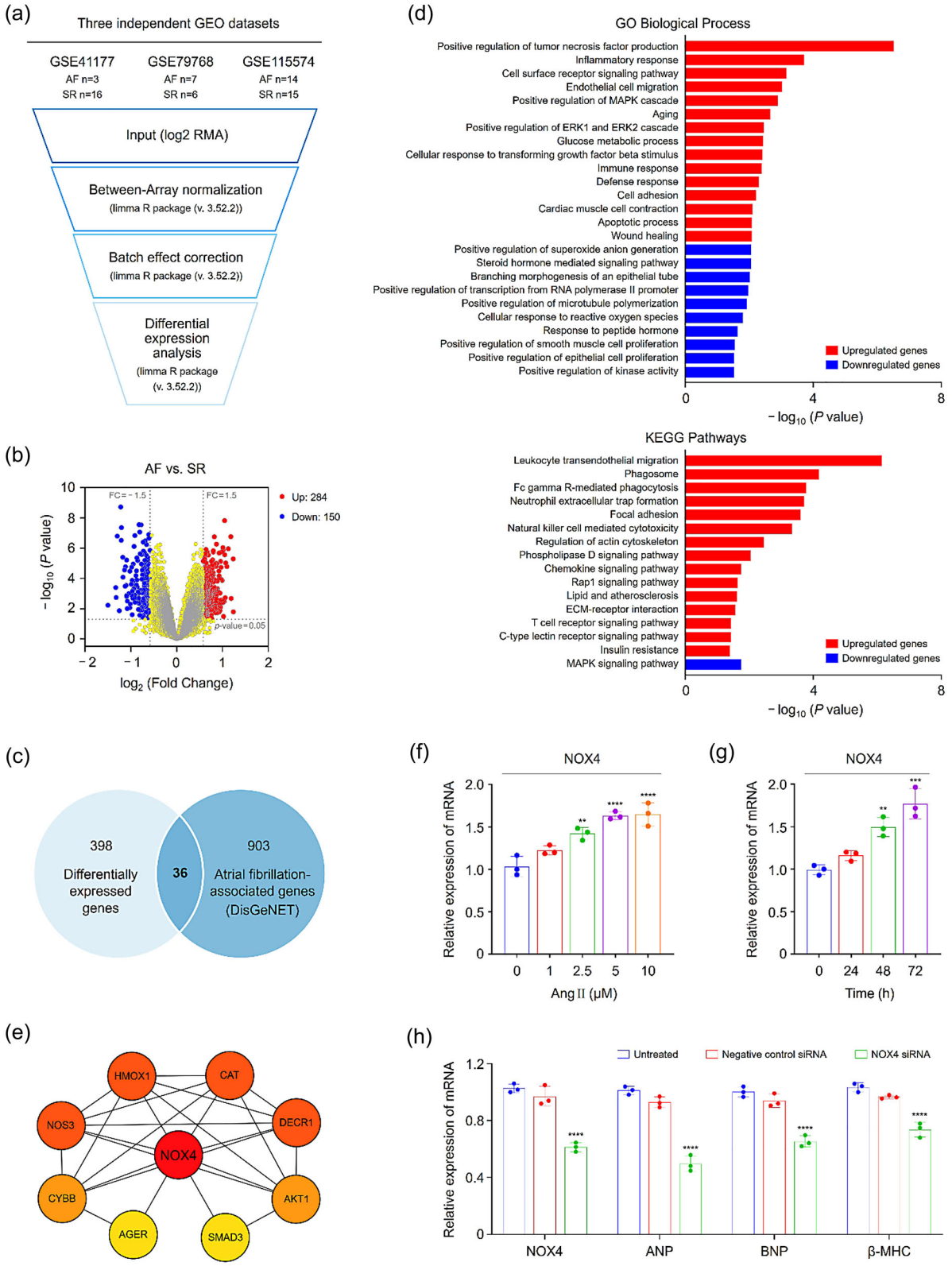

FIGURE 3 Investigation of a molecular target for treating cardiac hypertrophy. (a) Schematic diagram of in silico experimental design and analysis. (b) Volcano plot for a comparison of gene expression profiles between patients with SR and AF. The *x*-axis indicates the differential expression profiles, plotting the log2 (fold change). The *y*-axis indicates the statistical significance of differences. (c) Venn diagram showing overlapping areas between DEGs and AF-associated genes identified from DisGeNET. (d) GO and KEGG pathway enrichment analyses of selected 36 DEGs. (e) STRING PPI network of NOX4. (f and g) qRT-PCR analysis of NOX4 levels in iPSC-vCMs treated with Ang II at different concentrations and times. (h) qRT-PCR analysis of NOX4, ANP, BNP and β-MHC levels in the indicated groups. Data are normalized to GAPDH. $^{*}P < 0.05$, $^{**}P < 0.01$, $^{***}P < 0.001$, $^{****}P < 0.0001$.

responses. After iPSC-vCMs were treated with Ang II at different concentrations (1, 2.5, 5 and 10 μM) for 48 h, qRT-PCR analysis showed that mRNA levels of hypertrophic markers ANP, BNP and β-MHC were altered by Ang II treatment in a dose-dependent manner. In addition, treatment with 2.5 μM of Ang II significantly increased levels of these mRNAs in a time-dependent manner (Figure S7A and B). Thus, the concentration of 2.5 μM Ang II was selected for subsequent experiments. Consequently, Ang II treatment led to significant increase of NOX4 levels in a dose- and time-dependent manner (Figure 3f and g). Moreover, we confirmed that mRNA levels of ANP, BNP and β-MHC significantly decreased following knockdown of NOX4 (Figure 3h). Taken together, these results suggested that NOX4 functions as a positive regulator of cardiac hypertrophy.

3.4 | Targeted therapy of CEVs@siNOX4 in vitro

Based on these results, we expected that delivery of siNOX4 using CEVs would exert strong anti-hypertrophic effects. Hence, CEVs were loaded with cholesterol-modified siNOX4 as previously described (Figure 4a) (Tian et al., 2022; Zhang et al., 2019). As shown in Figure 4b–4e, there were no changes in the morphology, diameter, zeta potential and marker protein expression of CEVs@siNOX4, indicating that siNOX4 loading does not affect typical sEVs properties. In addition, IVIS fluorescence images showed a high accumulation of CEVs@siNOX4 in the heart, which was similar to the results obtained with CEVs (Figure 4f). Nevertheless, there was no marked difference in the fluorescence intensity of other organs (liver, spleen, lung and kidneys) between the groups (Figure S8). Therefore, these results demonstrated that the heart-targeting ability of CEVs was not affected by siNOX4 loading.

After preparing CEVs@siNOX4, we investigated whether CEVs could effectively load and deliver siNOX4 in vitro. The amount of siRNA was estimated by loading 5-carboxyfluorescein (FAM)-labelled siCtrl (with cholesterol modification) onto CEVs. Using a fluorescence standard curve of free FAM-labelled siCtrl, it was calculated that 100 μg/mL of CEVs@siCtrl contained 730 pmol siRNA, on average (Figure S9). Given that 100 μg/mL of the sEVs were incubated with 1 nmol siRNA at the beginning, the loading efficiency is approximately 73%. In addition, CEVs@siNOX4 significantly decreased the mRNA and protein levels of NOX4 in iPSC-vCMs, indicating that this knockdown was dependent on targeted delivery by CEVs (Figure 4g and h). Collectively, these results showed that CEVs efficiently contained siNOX4 and successfully delivered it to the cells.

Because the critical function of NOX4 is to induce cardiac hypertrophy, we explored the anti-hypertrophic effects of siNOX4 delivered by CEVs in Ang II-treated iPSC-vCMs. As shown in Figure 4i, Ang II treatment significantly increased mRNA levels of hypertrophic markers (ANP, BNP and β-MHC), whereas these changes were reversed by CEVs@siNOX4 treatment. In addition, the Ang II-induced increase in cardiomyocyte size was significantly reduced by treatment with CEVs@siNOX4 compared to the other groups (Figure 4j and k). Therefore, these in vitro results showed that CEVs@siNOX4 exerted an enhanced protective effect against Ang II-induced hypertrophic responses.

3.5 | Targeted therapy of CEVs@siNOX4 in vivo

Given its excellent in vitro therapeutic effects, we further evaluated in vivo anti-hypertrophic effects of CEVs@siNOX4. The mice were implanted with Ang II-containing osmotic pumps (or implanted with PBS-containing osmotic pumps as control) and 7 days later, intravenously injected with PBS, CEVs@siCtrl, SEVs@siNOX4, or CEVs@siNOX4. Each sample injection was repeated as shown in Figure 5a. Consequently, qRT-PCR analysis revealed that Ang II-induced NOX4 levels were significantly reversed by CEVs@siNOX4 injection, indicating that CEVs@siNOX4 successfully delivered siNOX4 to the mouse heart (Figure 5b). In addition, Ang II-treated group showed markedly increased heart weight/body weight ratio (HW/BW), fibrotic area and cardiomyocyte CSA compared to the control group; however, CEVs@siNOX4 injection resulted in a greater decrease in HW/BW, fibrotic area and cardiomyocyte CSA compared with CEV@siCtrl- or SEVs@siNOX4-injected groups, which can be attributed to the heart-targeted delivery of siNOX4 (Figure 5c–5h). Echocardiography showed that cardiac function (LVEF and LVFS) deteriorated in the Ang II-treated group; however, these changes were significantly reversed by CEVs@siNOX4 injection ($P < 0.05$; Figure 5i and 5j). Moreover, we found that mRNA levels of ANP, BNP and β-MHC significantly decreased by CEVs@siNOX4 injection as compared with those in the other two groups (Figure 5k). Finally, H&E-stained major organs (heart, liver, spleen, lung and kidneys) showed no obvious histological changes after systemic administration of the different treatments (Figure S10). Taken together, these results showed that CEVs@siNOX4 exerted a stronger targeted therapy for cardiac hypertrophy with good biocompatibility, thereby supporting its potential for clinical application in the treatment of cardiac hypertrophy.

4 | DISCUSSION

In this study, a sEV-based therapeutic nanoplatform for cardiac hypertrophy was designed; the platform possessed the following advantages: first, we selected human peripheral blood as the original source of sEVs. Several studies have shown that the yield

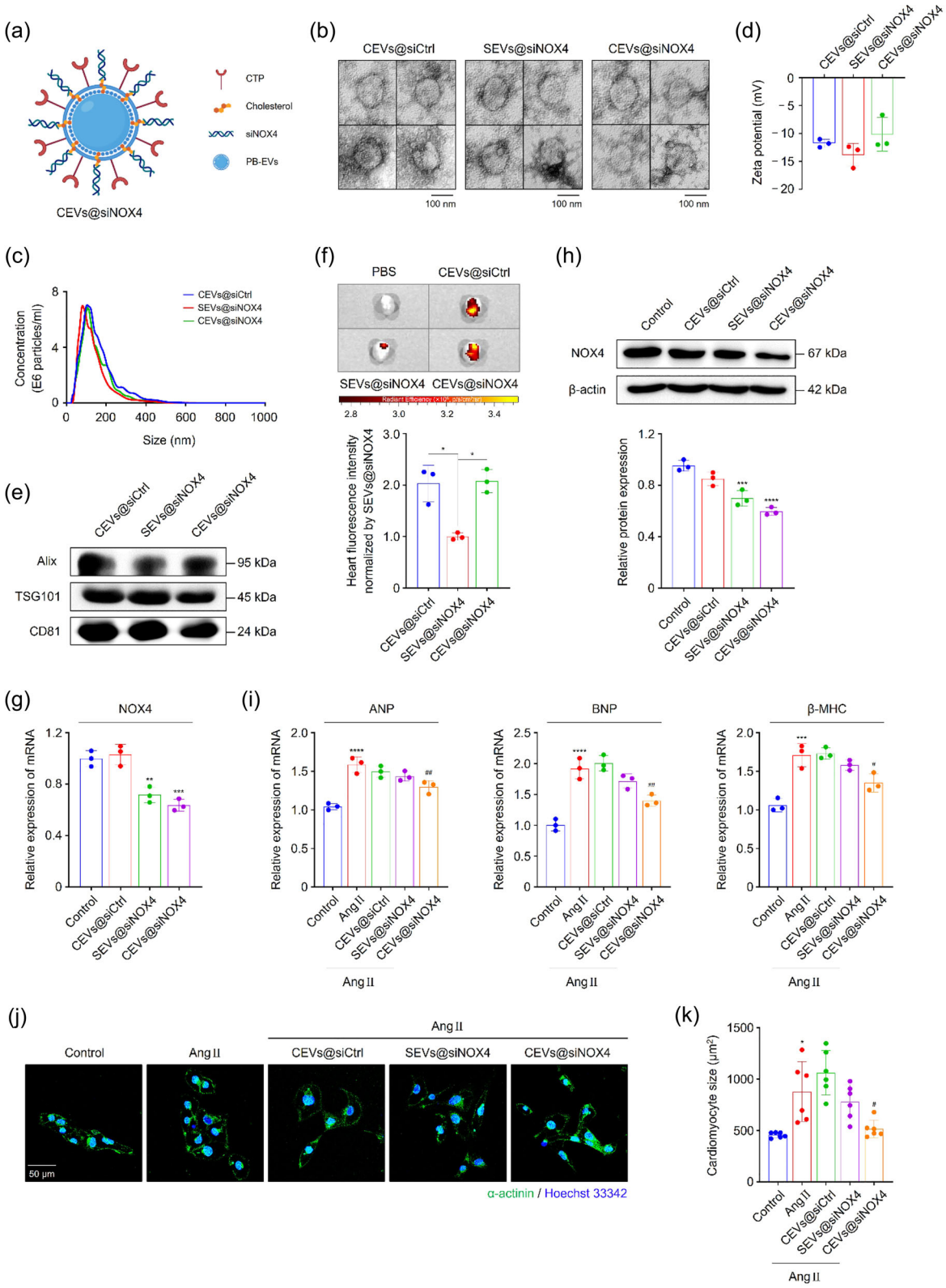

FIGURE 4 Characterization of CEVs@siNOX4 and its therapeutic effects in vitro. (a) Schematic diagram of siNOX4 loading onto CEVs. (B-D) Transmission electron micrograph (b), size distribution (c) and zeta potential analysis (d) of CEVs@siCtrl, SEVs@siNOX4 and CEVs@siNOX4. Scale bar = 100 nm. (e) Representative blots of Alix, TSG101 and CD81 in three types of sEVs. Uncropped blots are shown in Figure S11. (f) Representative IVIS images and quantified data showing fluorescence intensity in mice heart tissues 24 h after intravenous injection of PBS, CEVs@siCtrl, SEVs@siNOX4 or CEVs@siNOX4. (g) qRT-PCR analysis of NOX4 levels in iPSC-vCMs. Data are normalized to GAPDH. (h) Representative blots and quantified data showing NOX4 protein levels in the indicated groups. β-actin served as a loading control. Uncropped blots are shown in Figure S11. (i) qRT-PCR analysis of ANP, BNP and β-MHC levels in the indicated groups. Data are normalized to GAPDH. (j and k) Representative immunofluorescence images of α-actinin (green)- and Hoechst 33342 (blue)-stained iPSC-vCMs along with quantified data showing cardiomyocyte size. Scale bar = 50 μm. * Indicates comparison with the control group, $^{*}P < 0.05$, $^{**}P < 0.01$, $^{***}P < 0.001$, $^{****}P < 0.0001$; $^{\#}$ indicates comparison with the Ang II-treated group, $^{\#}P < 0.05$, $^{\#\#}P < 0.01$.

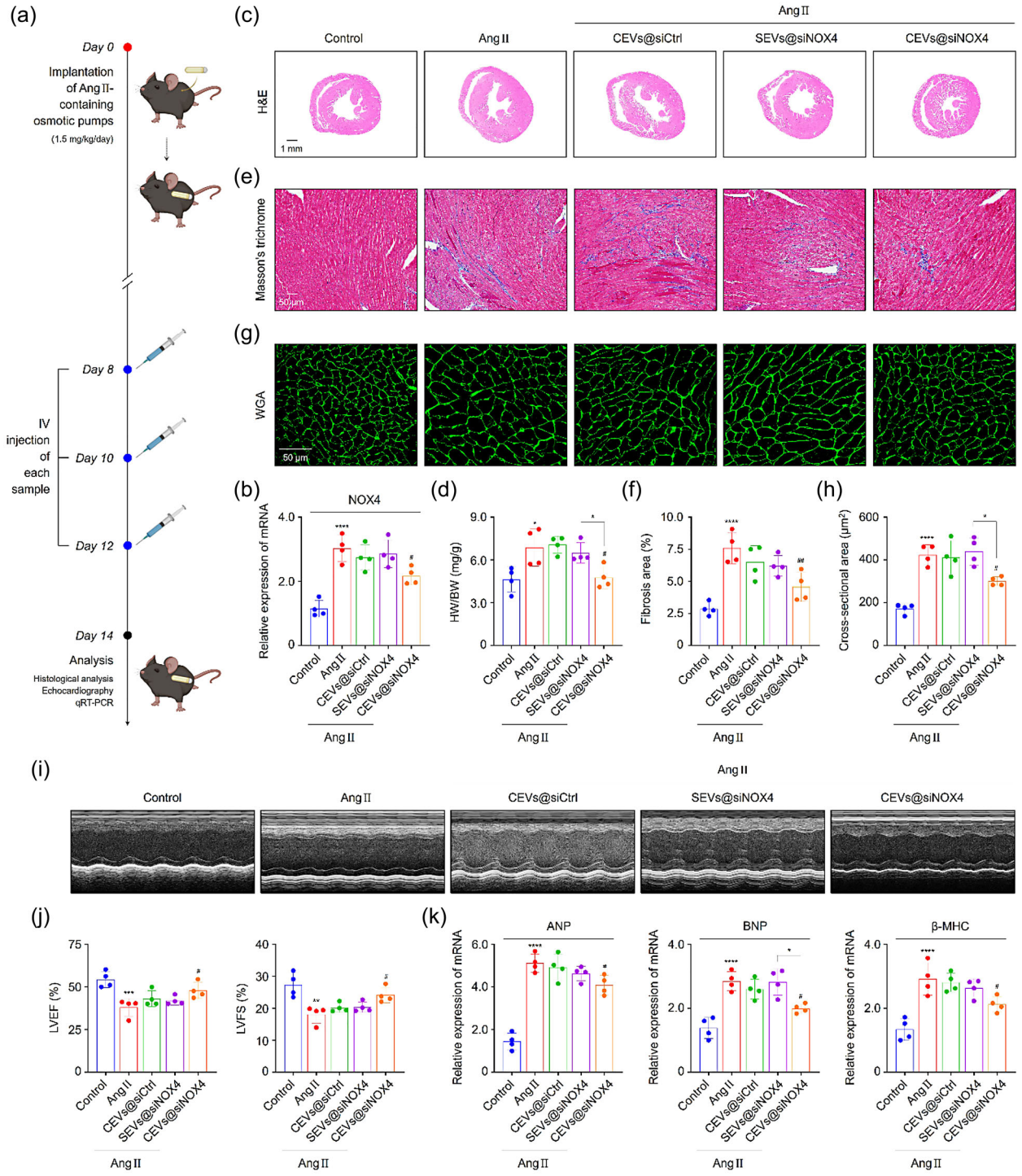

FIGURE 5 Therapeutic effects of CEVs@siNOX4 in vivo. (a) Schematic diagram of in vivo experimental design and analysis. (b) qRT-PCR analysis of NOX4 levels in mice heart tissues; $n = 4$ per group. Data are normalized to GAPDH. (c and d) Representative images of H&E-stained heart sections and quantified data showing HW/BW; $n = 4$ per group. Scale bar = 1 mm. (e and f) Representative images of MT-stained heart sections and quantified data showing fibrotic area (%); n = 4 per group. Scale bar = 50 μm. (g and h) Representative immunofluorescence images of WGA-stained heart sections and quantified data showing CSA; $n = 4$ per group. Scale bar = 50 μm. (i and j) Representative M-mode images (i) and quantified data showing LVEF and LVFS (j) in the indicated groups; $n = 4$ per group. (k) qRT-PCR analysis of ANP, BNP and β-MHC levels in the indicated groups; n = 4 per group. Data are normalized to GAPDH. * indicates comparison with the control group, $^{*}P < 0.05$, $^{**}P < 0.01$, $^{***}P < 0.001$, $^{****}P < 0.0001$; # indicates comparison with the Ang II-treated group, $^{\#}P < 0.05$, $^{\#\#}P < 0.01$.

of sEVs isolated from cell culture medium is usually very low, which limits their ability to obtain sufficient sEVs, thus severely impeding their wider application in research and clinical therapy (Usman et al., 2018; Xu et al., 2016). Although immortalized cells were used to isolate sEVs instead as to overcome this limitation, there is the risk of transferring oncogenic DNA and retrotransposon elements (Balaj et al., 2011). In comparison, human peripheral blood can be easily obtained from any human subject and has been used safely and routinely for blood transfusions. In addition, accumulated studies have demonstrated that PB-EVs act as efficient vehicles for drug delivery without obvious immunogenicity and toxicity in animal models (e.g., mice, rats and others) (Kang et al., 2019, 2020; Usman et al., 2018; Zhang et al., 2022; Zheng et al., 2022). Here, we expand these generic applications and demonstrate their remarkable extensibility; thus, we expect that PB-EVs could be used as an off-the-shelf therapy that enables efficient and specific delivery of siRNA for the treatment of cardiac hypertrophy.

Second, PB-EVs were modified with CTP, a peptide composed of 12-amino acids (APWHLSSQYSRT) that specifically targets cardiomyocytes (Avula et al., 2012, 2015; Zahid et al., 2010). Nguyen BY et al. have demonstrated that the capture of sEVs depends largely on the membrane compositions present on both the sEVs and the target cell (Nguyen et al., 2021). In fact, numerous studies have showed that sEVs conjugated with specific cell/tissue-targeting peptides are effectively taken up by target cells, eventually surpassing the natural uptake efficiency of individual cell types (Mentkowski & Lang, 2019; Vandergriff et al., 2018; Wang et al., 2018; Wei et al., 2021). Although fibroblasts and endothelial cells are known to take up sEVs more readily than cardiomyocytes, our in vitro and in vivo results showed a high uptake efficiency of CTP-modified functional sEVs by cardiomyocytes, compared to either endothelial cells or cardiac fibroblasts. Therefore, CEVs had strong tropism for cardiomyocytes and might serve as an efficient heart-targeted delivery system with safety and good biocompatibility. Moreover, we used a biochemical approach based on bio-orthogonal copper-free click chemistry for the easy and rapid modification of sEVs. Compared to cell engineering approaches, this efficient method is capable of conjugating various cell/tissue-targeting peptides to sEVs pre-isolated from cell culture medium or body fluids within 24 h (Tian et al., 2018). In addition, along with previous studies by other groups, we confirmed that bio-orthogonal copper-free click chemistry can be applied to living cells and mice without obvious toxicity (Baskin et al., 2007; Koo et al., 2012; Laughlin et al., 2008); thus, an advantage of this method is that it allows large-scale production of functionalized sEVs, thereby facilitating a continued supply of the nanocarrier.

Finally, cholesterol-conjugated siNOX4 was effectively loaded into CEVs through hydrophobic interactions and efficiently delivered to the heart. The delivery of CEVs@siNOX4 reversed Ang II-induced NOX4 expression and exerted cardioprotective effects both in vitro and in vivo. In particular, NOX4, a potential molecular target for treating cardiac hypertrophy, was inhibited by CEVs@siNOX4, and enhanced anti-hypertrophic effects were achieved because of CEVs with siNOX4 protection and heart-targeting ability. Therefore, our results not only suggest a practical strategy to overcome obstacles for heart-specific siRNA delivery, but also provide a promising tool for targeted therapy of cardiac hypertrophy.

In summary, our study suggests a targeting and treatment nanoplatform of siRNA based on CTP-modified functional sEVs, which has great potential for the treatment of cardiac hypertrophy and could be utilized as a promising strategy for the treatment of different types of cardiovascular diseases.

AUTHOR CONTRIBUTIONS

Ji-Young Kang: Conceptualization; Investigation; Validation; Writing—original draft. **Dasom Mun**: Investigation. **Yumin Chun**: Investigation. **Da-Seul Park**: Validation. **Hyoeun Kim**: Validation. **Nuri Yun**: Conceptualization; Supervision. **Boyoung Joung**: Conceptualization; Supervision.

ACKNOWLEDGEMENTS

This study was supported by the Korean Fund for Regenerative Medicine (KFRM) grant funded by the Korea government (the Ministry of Science and ICT (MSIT), the Ministry of Health & Welfare) (21B0604L1); the Basic Science Research Program through the National Research Foundation of Korea (NRF) funded by the Ministry of Education (2021R1I1A1A01052197); the NRF grant funded by the Korea government (MSIT) (2023R1A2C3003320); and the Korean Cardiac Research Foundation (202101-02). The authors would like to thank Editage (www.editage.co.kr) for English language editing, BioRender (www.biorender.com) for assistance with preparation of the figures, and the Bioinformatics Collaboration Unit (BiCU) at the Yonsei Biomedical Research Institute, Yonsei University College of Medicine.

CONFLICT OF INTEREST STATEMENT

The authors declare no conflict of interest.

ORCID

Boyoung Joung https://orcid.org/0000-0001-9036-7225

REFERENCES

Alvarez-Erviti, L., Seow, Y., Yin, H., Betts, C., Lakhal, S., & Wood, M. J. (2011). Delivery of siRNA to the mouse brain by systemic injection of targeted exosomes. *Nature biotechnology*, *29*(4), 341–345.

Armstrong, J. P., Holme, M. N., & Stevens, M. M. (2017). Re-engineering extracellular vesicles as smart nanoscale therapeutics. *ACS Nano*, *11*(1), 69–83.

Avula, U. M., Kim, G., Lee, Y. E., Morady, F., Kopelman, R., & Kalifa, J. (2012). Cell-specific nanoplatform-enabled photodynamic therapy for cardiac cells. *Heart Rhythm*, *9*(9), 1504–1509.

Avula, U. M., Yoon, H. K., Lee, C. H., Kaur, K., Ramirez, R. J., Takemoto, Y., Ennis, S. R., Morady, F., Herron, T., Berenfeld, O., Kopelman, R., & Kalifa, J. (2015). Cell-selective arrhythmia ablation for photomodulation of heart rhythm. *Science Translational Medicine*, *7*(311), 311ra172.

Balaj, L., Lessard, R., Dai, L., Cho, Y. J., Pomeroy, S. L., Breakefield, X. O., & Skog, J. (2011). Tumour microvesicles contain retrotransposon elements and amplified oncogene sequences. *Nature Communications*, *2*, 180.

Baskin, J. M., Prescher, J. A., Laughlin, S. T., Agard, N. J., Chang, P. V., Miller, I. A., Lo, A., Codelli, J. A., & Bertozzi, C. R. (2007). Copper-free click chemistry for dynamic in vivo imaging. *Proceedings of the National Academy of Sciences of the United States of America*, *104*(43), 16793–16797.

Berk, B. C., Fujiwara, K., & Lehoux, S. (2007). ECM remodeling in hypertensive heart disease. *The Journal of Clinical Investigation*, *117*(3), 568–575.

Colombo, M., Raposo, G., & Théry, C. (2014). Biogenesis, secretion, and intercellular interactions of exosomes and other extracellular vesicles. *Annual Review of Cell and Developmental Biology*, *30*, 255–289.

Cyganek, L., Tiburcy, M., Sekeres, K., Gerstenberg, K., Bohnenberger, H., Lenz, C., Henze, S., Stauske, M., Salinas, G., Zimmermann, W. H., Hasenfuss, G., & Guan, K. (2018). Deep phenotyping of human induced pluripotent stem cell-derived atrial and ventricular cardiomyocytes. *JCI Insight*, *3*(12), e99941.

De Jong, A. M., Maass, A. H., Oberdorf-Maass, S. U., Van Veldhuisen, D. J., Van Gilst, W. H., & Van Gelder, I. C. (2011). Mechanisms of atrial structural changes caused by stretch occurring before and during early atrial fibrillation. *Cardiovascular Research*, *89*(4), 754–765.

Dorn, G. W., 2nd, Robbins, J., & Sugden, P. H. (2003). Phenotyping hypertrophy: Eschew obfuscation. *Circulation Research*, *92*(11), 1171–1175.

El Andaloussi, S., Lakhal, S., Mäger, I., & Wood, M. J. (2013). Exosomes for targeted siRNA delivery across biological barriers. *Advanced Drug Delivery Reviews*, *65*(3), 391–397.

Frey, N., Katus, H. A., Olson, E. N., & Hill, J. A. (2004). Hypertrophy of the heart: A new therapeutic target? *Circulation*, *109*(13), 1580–1589.

Fu, L., Rao, F., Lian, F., Yang, H., Kuang, S., Wu, S., Deng, C., & Xue, Y. (2019). Mechanism of electrical remodeling of atrial myocytes and its influence on susceptibility to atrial fibrillation in diabetic rats. *Life Sciences*, *239*, 116903.

Goyal, B. R., Patel, M. M., Soni, M. K., & Bhadada, S. V. (2009). Therapeutic opportunities of small interfering RNA. *Fundamental & Clinical Pharmacology*, *23*(4), 367–386.

Hao, D., Lu, L., Song, H., Duan, Y., Chen, J., Carney, R., Li, J. J., Zhou, P., Nolta, J., Lam, K. S., Leach, J. K., Farmer, D. L., Panitch, A., & Wang, A. (2022). Engineered extracellular vesicles with high collagen-binding affinity present superior in situ retention and therapeutic efficacy in tissue repair. *Theranostics*, *12*(13), 6021–6037.

Hill, J. A. (2003). Electrical remodeling in cardiac hypertrophy. *Trends in Cardiovascular Medicine*, *13*(8), 316–322.

Hill, J. A., & Olson, E. N. (2008). Cardiac plasticity. *New England Journal of Medicine*, *358*(13), 1370–1380.

Iyer, S. S., & Cheng, G. (2012). Role of interleukin 10 transcriptional regulation in inflammation and autoimmune disease. *Critical Reviews in Immunology*, *32*(1), 23–63.

Jansen, H. J., Bohne, L. J., Gillis, A. M., & Rose, R. A. (2020). Atrial remodeling and atrial fibrillation in acquired forms of cardiovascular disease. *Heart Rhythm O2*, *1*(2), 147–159.

Kanasty, R., Dorkin, J. R., Vegas, A., & Anderson, D. (2013). Delivery materials for siRNA therapeutics. *Nature Materials*, *12*(11), 967–977.

Kang, J. Y., Kim, H., Mun, D., Yun, N., & Joung, B. (2020). Therapeutic potential of miR-21 regulation by human peripheral blood derived-small extracellular vesicles in myocardial infarction. *Clinical Science (London, England: 1979)*, *134*(8), 985–999.

Kang, J. Y., Park, H., Kim, H., Mun, D., Park, H., Yun, N., & Joung, B. (2019). Human peripheral bloodderived exosomes for microRNA delivery. *International Journal of Molecular Medicine*, *43*(6), 2319–2328.

Kim, H., Yun, N., Mun, D., Kang, J. Y., Lee, S. H., Park, H., Park, H., & Joung, B. (2018). Cardiac-specific delivery by cardiac tissue-targeting peptide-expressing exosomes. *Biochemical and Biophysical Research Communications*, *499*(4), 803–808.

Koo, H., Lee, S., Na, J. H., Kim, S. H., Hahn, S. K., Choi, K., Kwon, I. C., Jeong, S. Y., & Kim, K. (2012). Bioorthogonal copper-free click chemistry in vivo for tumor-targeted delivery of nanoparticles. *Angewandte Chemie (International ed. in English)*, *51*(47), 11836–11840.

Kooijmans, S. A. A., Schiffelers, R. M., Zarovni, N., & Vago, R. (2016). Modulation of tissue tropism and biological activity of exosomes and other extracellular vesicles: New nanotools for cancer treatment. *Pharmacological Research*, *111*, 487–500.

Kuroda, J., Ago, T., Matsushima, S., Zhai, P., Schneider, M. D., & Sadoshima, J. (2010). NADPH oxidase 4 (Nox4) is a major source of oxidative stress in the failing heart. *Proceedings of the National Academy of Sciences of the United States of America*, *107*(35), 15565–15570.

Lai, C. P., Mardini, O., Ericsson, M., Prabhakar, S., Maguire, C., Chen, J. W., Tannous, B. A., & Breakefield, X. O. (2014). Dynamic biodistribution of extracellular vesicles in vivo using a multimodal imaging reporter. *ACS Nano*, *8*(1), 483–494.

Lamberti, G., & Barba, A. A. (2020). Drug delivery of siRNA therapeutics. *Pharmaceutics*, *12*(2), 178.

Laughlin, S. T., Baskin, J. M., Amacher, S. L., & Bertozzi, C. R. (2008). In vivo imaging of membrane-associated glycans in developing zebrafish. *Science (New York, N.Y.)*, *320*(5876), 664–667.

Li, H., Xu, J. D., Fang, X. H., Zhu, J. N., Yang, J., Pan, R., Yuan, S. J., Zeng, N., Yang, Z. Z., Yang, H., Wang, X. P., Duan, J. Z., Wang, S., Luo, J. F., Wu, S. L., & Shan, Z. X. (2020). Circular RNA circRNA_000203 aggravates cardiac hypertrophy via suppressing miR-26b-5p and miR-140-3p binding to Gata4. *Cardiovascular Research*, *116*(7), 1323–1334.

Liang, S. F., Zuo, F. F., Yin, B. C., & Ye, B. C. (2022). Delivery of siRNA based on engineered exosomes for glioblastoma therapy by targeting STAT3. *Biomaterials Science*, *10*(6), 1582–1590.

Livak, K. J., & Schmittgen, T. D. (2001). Analysis of relative gene expression data using real-time quantitative PCR and the 2(-Delta Delta C(T)) Method. *Methods (San Diego, California)*, *25*(4), 402–408.

Lu, J., Sun, D., Liu, Z., Li, M., Hong, H., Liu, C., Gao, S., Li, H., Cai, Y., Chen, S., Li, Z., Ye, J., & Liu, P. (2016). SIRT6 suppresses isoproterenol-induced cardiac hypertrophy through activation of autophagy. *Translational Research: The Journal of Laboratory and Clinical Medicine*, *172*, 96–112.e6.

Lu, M., Xing, H., Xun, Z., Yang, T., Ding, P., Cai, C., Wang, D., & Zhao, X. (2018). Exosome-based small RNA delivery: Progress and prospects. *Asian Journal of Pharmaceutical Sciences*, *13*(1), 1–11.

Ma, Y., Huang, H., Jiang, J., Wu, L., Lin, C., Tang, A., Dai, G., He, J., & Chen, Y. (2016). AVE 0991 attenuates cardiac hypertrophy through reducing oxidative stress. *Biochemical and Biophysical Research Communications*, *474*(4), 621–625.

Maas, R. G. C., Lee, S., Harakalova, M., Snijders Blok, C. J. B., Goodyer, W. R., Hjortnaes, J., Doevendans, P. A. F. M., Van Laake, L. W., van der Velden, J., Asselbergs, F. W., Wu, J. C., Sluijter, J. P. G., Wu, S. M., & Buikema, J. W. (2021). Massive expansion and cryopreservation of functional human induced pluripotent stem cell-derived cardiomyocytes. *STAR Protocols*, *2*(1), 100334.

MacIntyre, C., & Lakdawala, N. K. (2016). Management of atrial fibrillation in hypertrophic cardiomyopathy. *Circulation*, *133*(19), 1901–1905.

Mathivanan, S., Ji, H., & Simpson, R. J. (2010). Exosomes: Extracellular organelles important in intercellular communication. *Journal of Proteomics*, *73*(10), 1907–1920.

Matsushima, S., Kuroda, J., Ago, T., Zhai, P., Park, J. Y., Xie, L. H., Tian, B., & Sadoshima, J. (2013). Increased oxidative stress in the nucleus caused by Nox4 mediates oxidation of HDAC4 and cardiac hypertrophy. *Circulation Research*, *112*(4), 651–663.

Mentkowski, K. I., & Lang, J. K. (2019). Exosomes engineered to express a cardiomyocyte binding peptide demonstrate improved cardiac retention in vivo. *Scientific Reports*, *9*(1), 10041.

Murphy, D. E., de Jong, O. G., Brouwer, M., Wood, M. J., Lavieu, G., Schiffelers, R. M., & Vader, P. (2019). Extracellular vesicle-based therapeutics: Natural versus engineered targeting and trafficking. *Experimental & Molecular Medicine*, *51*(3), 1–12.

Nguyen, B. Y., Azam, T., & Wang, X. (2021). Cellular signaling cross-talk between different cardiac cell populations: An insight into the role of exosomes in the heart diseases and therapy. *American Journal of Physiology. Heart and Circulatory Physiology*, *320*(4), H1213–H1234.

Poller, W., Tank, J., Skurk, C., & Gast, M. (2013). Cardiovascular RNA interference therapy: The broadening tool and target spectrum. *Circulation Research*, *113*(5), 588–602.

Raghunathan, S., & Patel, B. M. (2013). Therapeutic implications of small interfering RNA in cardiovascular diseases. *Fundamental & Clinical Pharmacology*, *27*(1), 1–20.

Ramasubramanian, L., Kumar, P., & Wang, A. (2019). Engineering extracellular vesicles as nanotherapeutics for regenerative medicine. *Biomolecules*, *10*(1), 48.

Reischl, D., & Zimmer, A. (2009). Drug delivery of siRNA therapeutics: Potentials and limits of nanosystems. *Nanomedicine: Nanotechnology, Biology, and Medicine*, *5*(1), 8–20.

Ritchie, M. E., Phipson, B., Wu, D., Hu, Y., Law, C. W., Shi, W., & Smyth, G. K. (2015). limma powers differential expression analyses for RNA-sequencing and microarray studies. *Nucleic Acids Research*, *43*(7), e47.

Rosenberg, M. A., Das, S., Quintero Pinzon, P., Knight, A. C., Sosnovik, D. E., Ellinor, P. T., & Rosenzweig, A. (2012). A novel transgenic mouse model of cardiac hypertrophy and atrial fibrillation. *Journal of Atrial Fibrillation*, *4*(5), 415.

Ruwhof, C., & van der Laarse, A. (2000). Mechanical stress-induced cardiac hypertrophy: Mechanisms and signal transduction pathways. *Cardiovascular Research*, *47*(1), 23–37.

Schoenborn, J. R., & Wilson, C. B. (2007). Regulation of interferon-gamma during innate and adaptive immune responses. *Advances in Immunology*, *96*, 41–101.

Schoonderwoerd, B. A., Van Gelder, I. C., Van Veldhuisen, D. J., Van den Berg, M. P., & Crijns, H. J. (2005). Electrical and structural remodeling: Role in the genesis and maintenance of atrial fibrillation. *Progress in Cardiovascular Diseases*, *48*(3), 153–168.

Shah, A. M., & Giacca, M. (2022). Small non-coding RNA therapeutics for cardiovascular disease. *European Heart Journal*, *43*(43), 4548–4561.

Shah, R., Patel, T., & Freedman, J. E. (2018). Circulating extracellular vesicles in human disease. *The New England Journal of Medicine*, *379*(10), 958–966.

Shimizu, I., & Minamino, T. (2016). Physiological and pathological cardiac hypertrophy. *Journal of Molecular and Cellular Cardiology*, *97*, 245–262.

Tanaka, T., Narazaki, M., & Kishimoto, T. (2014). IL-6 in inflammation, immunity, and disease. *Cold Spring Harbor Perspectives in Biology*, *6*(10), a016295.

Tatiparti, K., Sau, S., Kashaw, S. K., & Iyer, A. K. (2017). siRNA delivery strategies: A comprehensive review of recent developments. *Nanomaterials (Basel, Switzerland)*, *7*(4), 77.

Théry, C., Witwer, K. W., Aikawa, E., Alcaraz, M. J., Anderson, J. D., Andriantsitohaina, R., Antoniou, A., Arab, T., Archer, F., Atkin-Smith, G. K., Ayre, D. C., Bach, J. M., Bachurski, D., Baharvand, H., Balaj, L., Baldacchino, S., Bauer, N. N., Baxter, A. A., Bebawy, M., … & Zuba-Surma, E. K. (2018). Minimal information for studies of extracellular vesicles 2018 (MISEV2018): A position statement of the International Society for Extracellular Vesicles and update of the MISEV2014 guidelines. *Journal of Extracellular Vesicles*, *7*(1), 1535750.

Théry, C., Zitvogel, L., & Amigorena, S. (2002). Exosomes: Composition, biogenesis and function. *Nature Reviews. Immunology*, *2*(8), 569–579.

Tian, T., Liang, R., Erel-Akbaba, G., Saad, L., Obeid, P. J., Gao, J., Chiocca, E. A., Weissleder, R., & Tannous, B. A. (2022). Immune checkpoint inhibition in GBM primed with radiation by engineered extracellular vesicles. *ACS Nano*, *16*(2), 1940–1953.

Tian, T., Zhang, H. X., He, C. P., Fan, S., Zhu, Y. L., Qi, C., Huang, N. P., Xiao, Z. D., Lu, Z. H., Tannous, B. A., & Gao, J. (2018). Surface functionalized exosomes as targeted drug delivery vehicles for cerebral ischemia therapy. *Biomaterials*, *150*, 137–149.

Usman, W. M., Pham, T. C., Kwok, Y. Y., Vu, L. T., Ma, V., Peng, B., Chan, Y. S., Wei, L., Chin, S. M., Azad, A., He, A. B., Leung, A. Y. H., Yang, M., Shyh-Chang, N., Cho, W. C., Shi, J., & Le, M. T. N. (2018). Efficient RNA drug delivery using red blood cell extracellular vesicles. *Nature Communications*, *9*(1), 2359.

Vader, P., Mol, E. A., Pasterkamp, G., & Schiffelers, R. M. (2016). Extracellular vesicles for drug delivery. *Advanced Drug Delivery Reviews*, *106*(Pt A), 148–156.

Vandergriff, A., Huang, K., Shen, D., Hu, S., Hensley, M. T., Caranasos, T. G., Qian, L., & Cheng, K. (2018). Targeting regenerative exosomes to myocardial infarction using cardiac homing peptide. *Theranostics*, *8*(7), 1869–1878.

Walker, S., Busatto, S., Pham, A., Tian, M., Suh, A., Carson, K., Quintero, A., Lafrence, M., Malik, H., Santana, M. X., & Wolfram, J. (2019). Extracellular vesicle-based drug delivery systems for cancer treatment. *Theranostics*, *9*(26), 8001–8017.

Wang, J., Hu, L., Huang, H., Yu, Y., Wang, J., Yu, Y., Li, K., Li, Y., Tian, T., & Chen, F. (2020). CAR (CARSKNKDC) peptide modified rencell-derived extracellular vesicles as a novel therapeutic agent for targeted pulmonary hypertension therapy. *Hypertension (Dallas, Tex.: 1979)*, *76*(4), 1147–1160.

Wang, X., Chen, Y., Zhao, Z., Meng, Q., Yu, Y., Sun, J., Yang, Z., Chen, Y., Li, J., Ma, T., Liu, H., Li, Z., Yang, J., & Shen, Z. (2018). Engineered exosomes with ischemic myocardium-targeting peptide for targeted therapy in myocardial infarction. *Journal of the American Heart Association*, *7*(15), e008737.

Wei, Z., Chen, Z., Zhao, Y., Fan, F., Xiong, W., Song, S., Yin, Y., Hu, J., Yang, K., Yang, L., Xu, B., & Ge, J. (2021). Mononuclear phagocyte system blockade using extracellular vesicles modified with CD47 on membrane surface for myocardial infarction reperfusion injury treatment. *Biomaterials*, *275*, 121000.

Whitehead, K. A., Langer, R., & Anderson, D. G. (2009). Knocking down barriers: Advances in siRNA delivery. *Nature Reviews. Drug Discovery*, *8*(2), 129–138.

Wiklander, O. P., Nordin, J. Z., O'Loughlin, A., Gustafsson, Y., Corso, G., Mäger, I., Vader, P., Lee, Y., Sork, H., Seow, Y., Heldring, N., Alvarez-Erviti, L., Smith, C. I., Le Blanc, K., Macchiarini, P., Jungebluth, P., Wood, M. J., & Andaloussi, S. E. (2015). Extracellular vesicle in vivo biodistribution is determined by cell source, route of administration and targeting. *Journal of Extracellular Vesicles*, *4*, 26316.

Xu, R., Greening, D. W., Zhu, H. J., Takahashi, N., & Simpson, R. J. (2016). Extracellular vesicle isolation and characterization: Toward clinical application. *The Journal of Clinical Investigation*, *126*(4), 1152–1162.

Yang, S., Wang, J., Brand, D. D., & Zheng, S. G. (2018). Role of TNF-TNF receptor 2 signal in regulatory T cells and its therapeutic implications. *Frontiers in Immunology*, *9*, 784.

Yang, Y., Du, J., Xu, R., Shen, Y., Yang, D., Li, D., Hu, H., Pei, H., & Yang, Y. (2020). Melatonin alleviates angiotensin-II-induced cardiac hypertrophy via activating MICU1 pathway. *Aging*, *13*(1), 493–515.

Zahid, M., Phillips, B. E., Albers, S. M., Giannoukakis, N., Watkins, S. C., & Robbins, P. D. (2010). Identification of a cardiac specific protein transduction domain by in vivo biopanning using a M13 phage peptide display library in mice. *PLoS One*, *5*(8), e12252.

Zeng, S. Y., Yang, L., Lu, H. Q., Yan, Q. J., Gao, L., & Qin, X. P. (2019). Rutaecarpine prevents hypertensive cardiac hypertrophy involving the inhibition of Nox4-ROS-ADAM17 pathway. *Journal of Cellular and Molecular Medicine*, *23*(6), 4196–4207.

Zhang, H., Wu, J., Wu, J., Fan, Q., Zhou, J., Wu, J., Liu, S., Zang, J., Ye, J., Xiao, M., Tian, T., & Gao, J. (2019). Exosome-mediated targeted delivery of miR-210 for angiogenic therapy after cerebral ischemia in mice. *Journal of Nanobiotechnology*, *17*(1), 29.

Zhang, J., Ji, C., Zhang, H., Shi, H., Mao, F., Qian, H., Xu, W., Wang, D., Pan, J., Fang, X., Santos, H. A., & Zhang, X. (2022). Engineered neutrophil-derived exosome-like vesicles for targeted cancer therapy. *Science Advances*, *8*(2), eabj8207.

Zheng, G., Ma, H. W., Xiang, G. H., He, G. L., Cai, H. C., Dai, Z. H., Chen, Y. L., Lin, Y., Xu, H. Z., Ni, W. F., Xu, C., Liu, H. X., & Wang, X. Y. (2022). Bone-targeting delivery of platelet lysate exosomes ameliorates glucocorticoid-induced osteoporosis by enhancing bone-vessel coupling. *Journal of Nanobiotechnology*, *20*(1), 220.

Zhu, L. P., Tian, T., Wang, J. Y., He, J. N., Chen, T., Pan, M., Xu, L., Zhang, H. X., Qiu, X. T., Li, C. C., Wang, K. K., Shen, H., Zhang, G. G., & Bai, Y. P. (2018). Hypoxia-elicited mesenchymal stem cell-derived exosomes facilitates cardiac repair through miR-125b-mediated prevention of cell death in myocardial infarction. *Theranostics*, *8*(22), 6163–6177.

Zhu, Z., Zhai, Y., Hao, Y., Wang, Q., Han, F., Zheng, W., Hong, J., Cui, L., Jin, W., Ma, S., Yang, L., & Cheng, G. (2022). Specific anti-glioma targeted-delivery strategy of engineered small extracellular vesicles dual-functionalised by Angiopep-2 and TAT peptides. *Journal of Extracellular Vesicles*, *11*(8), e12255.

Zu, H., & Gao, D. (2021). Non-viral vectors in gene therapy: recent development, challenges, and prospects. *The AAPS Journal*, *23*(4), 78.

SUPPORTING INFORMATION

Additional supporting information can be found online in the Supporting Information section at the end of this article.

How to cite this article: Kang, J.-Y., Mun, D., Chun, Y., Park, D.-S., Kim, H., Yun, N., & Joung, B. (2023). Engineered small extracellular vesicle-mediated NOX4 siRNA delivery for targeted therapy of cardiac hypertrophy. *Journal of Extracellular Vesicles*, *12,* e12371. https://doi.org/10.1002/jev2.12371